J Biomol NMR (2011) 51:191–198
DOI 10.1007/s10858-011-9553-x

ARTICLE

Simultaneous measurement of ^{1}H–^{15}N and Methyl $^{1}H_m$–$^{13}C_m$ residual dipolar couplings in large proteins

Xinli Liao · Raquel Godoy-Ruiz · Chenyun Guo · Vitali Tugarinov

Received: 18 May 2011 / Accepted: 30 June 2011

Abstract A two-dimensional TROSY-based SIM-$^{13}C_m$–$^{1}H_m$/^{1}H–^{15}N NMR experiment for simultaneous measurements of methyl $^{1}D_{CH}$ and backbone amide $^{1}D_{NH}$ residual dipolar couplings (RDC) in {U-[^{15}N,^{2}H]; Ileδ1-[$^{13}CH_3$]; Leu,Val-[$^{13}CH_3$/$^{12}CD_3$]}-labeled samples of large proteins is described. Significant variation in the alignment tensor of the 82-kDa enzyme Malate synthase G is observed as a function of only slight changes in experimental conditions. The SIM-$^{13}C_m$–$^{1}H_m$/^{1}H–^{15}N data sets provide convenient means of establishing the alignment tensor characteristics via the measurement of $^{1}D_{NH}$ RDCs in the same protein sample.

Keywords Transverse relaxation optimized spectroscopy (TROSY) · Residual dipolar coupling (RDC) · Alignment tensor · Malate synthase G (MSG)

The knowledge of accurate parameters of an alignment tensor is paramount for interpretation of residual dipolar couplings (RDCs; Tjandra and Bax 1997; Tolman et al. 1995) in terms of protein structure (Bax et al. 2001; Prestegard 1998). The interpretation of methyl RDCs is additionally complicated by the dynamics of side chains on a variety of time-scales that cannot be quantitatively accounted for by scaling the 'static' RDC values with the methyl three-fold rotation axis order parameter, S_{axis}. Because of mobility of methyl-bearing side-chains $^{1}H_m$–$^{13}C_m$ methyl RDCs ($^{1}D_{CH}$) are extremely unreliable probes for derivation of alignment tensor characteristics. Although $^{1}D_{CH}$ couplings in usually more ordered alanine methyls may constitute an exception (Godoy-Ruiz et al. 2010), the number of Ala$^{\beta}$ methyl probes in large multi-domain protein structures can be insufficient for reliable estimates of the alignment parameters. Since for optimal sensitivity and resolution, methyl-TROSY-based NMR measurements of large proteins are usually conducted in D_2O (Tugarinov et al. 2003), alignment tensor characteristics have to be either measured separately from backbone amide ^{1}H-^{15}N RDCs ($^{1}D_{NH}$) or (if such data is not available) predicted from the structure of the protein molecule (Sprangers and Kay 2007).

The present study has been stimulated by the difficulties in interpretation of methyl $^{1}D_{CH}$ RDCs in a number of pf1-phage-oriented (Hansen et al. 1998) {U-[^{15}N,^{2}H]; Ileδ1-[$^{13}CH_3$]; Leu,Val-[$^{13}CH_3$/$^{12}CD_3$]}-labeled 82-kDa monomeric enzyme Malate synthase G (MSG) using alignment tensor parameters that have been obtained earlier from the measurements of $^{1}D_{NH}$ RDCs in U-[^{15}N,^{13}C,^{2}H]-labeled samples (Tugarinov and Kay 2003). Keeping in mind that even slight changes in experimental conditions (exact degree of alignment, ionic strength, pH, etc.) can significantly affect alignment parameters, we have turned to simultaneous measurements of the backbone $^{1}D_{NH}$ and methyl $^{1}D_{CH}$ RDCs in the samples of MSG dissolved in H_2O with the purpose of accurate determination of the alignment tensor from the backbone $^{1}D_{NH}$ data and then using this information for analysis of the structural information encoded in methyl RDCs. We show on the example

Xinli Liao is on leave from the Department of Chemistry, Xiamen University, China.

Electronic supplementary material The online version of this article (doi:10.1007/s10858-011-9553-x) contains supplementary material, which is available to authorized users.

X. Liao · R. Godoy-Ruiz · C. Guo · V. Tugarinov (✉)
Department of Chemistry and Biochemistry, University of Maryland, College Park, MD 20742, USA
e-mail: vitali@umd.edu

of MSG that alignment tensors can differ significantly even between samples prepared under practically identical experimental conditions. Two main advantages of simultaneous as opposed to sequential RDC measurements can be envisaged. First, it is the convenience of recording ^{1}H–^{15}N and methyl ^{1}H–^{13}C correlation maps in a single experiment—especially when the structure of a large protein is probed by RDC's as a function of ligand/substrate binding that would involve a series of RDC measurements. Second, protein samples may prove unstable in a number of weak alignment media. Clearly, instabilities in protein samples affect both backbone amide ^{1}H–^{15}N and methyl RDCs to the same extent if RDC measurements are conducted simultaneously. Alignment tensor parameters can thus be derived from the set of $^{1}D_{\mathrm{NH}}$ couplings under exactly the same experimental conditions.

Recently, we have introduced a TROSY-based (Pervushin et al. 1997; Tugarinov et al. 2003) 2D pulse-scheme for simultaneous (time-shared) detection of amide (^{1}H–^{15}N) and methyl (^{1}H$_{\mathrm{m}}$–^{13}C$_{\mathrm{m}}$) correlation maps in large perdeuterated protein samples uniformly isotope labeled with ^{15}N and selectively labeled with ^{13}CH$_3$ methyl groups at Ileδ1, Valγ and Leuδ (ILV) positions (Guo et al. 2008). This experiment has been designed to preserve the slowly relaxing components of both backbone ^{1}H–^{15}N amide and methyl ^{13}CH$_3$ spin-systems in the course of indirect evolution (t_1) and direct detection (t_2) periods, and has been applied to the studies of substrate binding to {U-[^{15}N,^{2}H]; Ileδ1-[^{13}CH$_3$]; Leu,Val-[^{13}CH$_3$/^{12}CD$_3$]}-labeled MSG (Guo et al. 2008). Although optimal acquisition of simultaneous ^{13}C$_{\mathrm{m}}$–^{1}H$_{\mathrm{m}}$/^{1}H–^{15}N 2D correlation maps is more a matter of convenience rather than gains in signal-to-noise or resolution of NMR spectra, this methodology has found an application in HN-methyl NOESY experiments (Guo and Tugarinov 2009). The time-shared amide-methyl detection scheme can be adapted in a relatively straightforward manner to simultaneous measurements of $^{1}D_{\mathrm{NH}}$ and $^{1}D_{\mathrm{CH}}$ RDCs in large proteins.

Figure 1 shows a pulse scheme for a 2D SIM-^{13}C$_{\mathrm{m}}$–^{1}H$_{\mathrm{m}}$/^{1}H–^{15}N experiment that we used for simultaneous measurements of $^{1}D_{\mathrm{CH}}$ and $^{1}D_{\mathrm{NH}}$ couplings in {U-[^{15}N,^{2}H]; Ileδ1-[^{13}CH$_3$]; Leu,Val-[^{13}CH$_3$/^{12}CD$_3$]}-labeled MSG dissolved in H_2O. Because the central (slowly-decaying) component of ^{1}H–^{13}C multiple-quantum methyl triplet does not evolve due to ^{1}H–^{13}C J couplings, $^{1}D_{\mathrm{CH}}$ in ^{13}CH$_3$ groups of large proteins have to be measured using the IPAP principle (Ottiger et al. 1998a, b; Yang and Nagayama 1996) from the F_2 dimension where methyl magnetization is in the single-quantum state (Sprangers and Kay 2007; Velyvis et al. 2009). Amide $^{1}D_{\mathrm{NH}}$ RDCs can be measured in the F_1 (indirect; ^{15}N) dimension of simultaneous ^{13}C$_{\mathrm{m}}$–^{1}H$_{\mathrm{m}}$/^{1}H–^{15}N 2D spectra from the splitting between the TROSY and ^{1}H-decoupled ^{15}N components (Kontaxis et al. 2000; Tugarinov and Kay 2003; Yang et al. 1999). Two experiments are performed for isotropic and aligned protein samples: (1) with the last two ^{13}C pulses shown with open rectangles in Fig. 1, *included* and the ^{1}H pulse in the middle of t_1 period implemented as a phase-modulated 180° refocusing pulse selective for methyl ^{1}H signals. This provides in-phase (IP) doublets in the methyl region and ^{1}H–^{15}N TROSY correlations in the amide region of the spectrum; (2) with the last two 'open' ^{13}C pulses *omitted*, the ^{1}H pulse in the middle of t_1 period implemented as a hard 180° refocusing pulse applied at the ^{1}H carrier frequency (water signal), with concomitant inversion of the phase of the second ^{1}H 180° SNEEZE pulse immediately following the t_1 period (ϕ4). This provides anti-phase (AP) methyl doublets and ^{1}H-decoupled amide ^{15}N correlations in the amide region of the 2D correlation map. Subsequently, the amide and methyl regions of the spectra are processed separately: methyl IP and AP sub-spectra are added and subtracted to produce singlets separated in F_2 by $^{1}J_{\mathrm{CH}}$ and ($^{1}J_{\mathrm{CH}} + {}^{1}D_{\mathrm{CH}}$) in the isotropic(aligned) samples, whereas amide TROSY and ^{1}H-decoupled subspectra can be used directly for the measurements of $^{1}J_{\mathrm{CH}}$ and ($^{1}J_{\mathrm{CH}} + {}^{1}D_{\mathrm{CH}}$) couplings.

Active suppression of ^{15}N anti-TROSY components is achieved in both experiments by including the filter between ^{15}N$_{\phi 1}$ and ^{15}N$_{\phi 2}$ pulses and shifting the phases of the ^{15}N$_{\phi 2}$ and ^{15}N$_{\phi 5}$ pulses by 45° (Fig. 1; Yang and Kay 1999). Although this is not necessary for the first dataset where the ^{1}H–^{15}N TROSY components are observed, if active suppression is not employed in the second (^{1}H-decoupled) experiment, the fast-relaxing ^{15}N doublet component during the first half of the t_1 period will be converted to and evolve as a slowly-relaxing signal during the second half of the t_1 period and will become visible in the spectra at the ^{1}H frequency of $+J_{\mathrm{NH}}$ relative to the chemical shift of the ^{1}H-decoupled component in F_2. Of note, in agreement with previous observations (Guo et al. 2008), the ^{1}H–^{15}N TROSY selecting version of the SIM-^{13}C$_{\mathrm{m}}$–^{1}H$_{\mathrm{m}}$/^{1}H–^{15}N experiment is on average ~35% less sensitive than individual ^{1}H–^{15}N TROSY (Pervushin et al. 1998) and HMQC-IPAP (Sprangers and Kay 2007) experiments recorded on MSG in H_2O (37°C). However, considering that a factor of two in acquisition time is saved by recording the two correlation maps simultaneously, this translates to approximately the same sensitivity per unit of time. The advantage of recording methyl-TROSY spectra (Tugarinov et al. 2003) in D_2O with optimal sensitivity is therefore 'traded' here for the convenience of simultaneous measurement of ^{1}H–^{15}N and ^{13}C$_{\mathrm{m}}$–^{1}H$_{\mathrm{m}}$ RDCs in the same protein sample and under exactly the same experimental conditions.

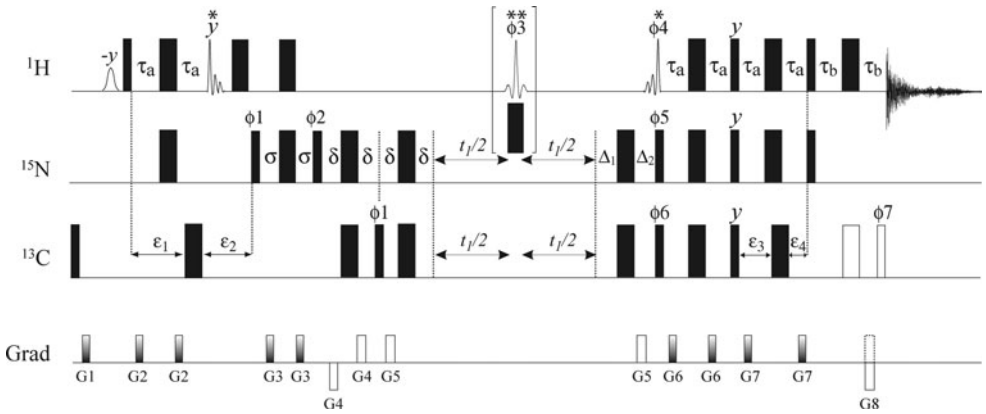

Fig. 1 Simultaneous ^{1}H–^{15}N/^{13}CH$_3$ pulse scheme (2D SIM-^{13}C$_m$–^{1}H$_m$/^{15}N–^{1}HN) for the measurements of ^{1}H–^{15}N and methyl ^{1}H$_m$–^{13}C$_m$ RDCs in large proteins. All narrow (*wide*) rectangular pulses are applied with flip angles of 90 (180)° along the *x*-axis unless indicated otherwise. The ^{1}H, ^{15}N and ^{13}C carrier frequencies are positioned at 4.7, 119, and 23 ppm, respectively. The first water-selective ^{1}H pulse has an E-BURP-1 shape (Geen and Freeman 1991) and duration of 7 ms. Two ^{1}H pulses marked with *asterisks* are 1.25 ms time-reversed SNEEZE (phase *y*) and SNEEZE shapes (Nuzillard and Freeman 1994), respectively, (600 MHz) with the center of excitation shifted to 8 ppm via phase modulation of RF field (Boyd and Soffe 1989; Patt 1992) for excitation of amide protons and the water signal. The pulse marked with *double asterisks* ($\phi 3$) is a 1.25 ms RE-BURP pulse (Geen and Freeman 1991) centered at −1.1 ppm via phase modulation of RF field for selective refocusing of methyl protons in experiment (1) and a hard pulse 180° centered on the water resonance in experiment (2). ^{13}C pulses shown with *open rectangles* are applied only in experiment (1)—see text. Note that the methyl and the amide regions of the ^{1}H-decoupled spectra (experiment 2) cannot be simultaneously phased to absorption mode in the direct acquisition dimension (F_2), and should be separated post-acquisition into individual sub-spectra and phased separately (see text). Delays are: $\tau_a = 2.3$ ms; $\tau_b = 2$ ms; $\sigma = 1.33$ ms; $\delta = 0.5$ ms; $\varepsilon_1 = 3.1$ ms; $\varepsilon_2 = 2.5$ ms; $\varepsilon_3 = 2.6$ ms; $\varepsilon_4 = 2.0$ ms. Delays Δ_i are carefully adjusted to avoid the evolution of methyl ^{1}H chemical shifts before and during t_1 period: $\Delta_1 = 3\delta + \mathrm{pw_N}$; $\Delta_2 = 3\delta + \mathrm{pw_N} + \mathrm{P}_{\phi 3}$, where $\mathrm{pw_N}$ is the length of nitrogen pulse, and $\mathrm{P}_{\phi 3}$ is the length of the RE-BURP pulse in experiment (1) and the hard 180° ^{1}H pulse in experiment (2). Durations and strengths of pulsed-field gradients in units of (ms; G/cm) are: G1 = (1; 15); G2 = (0.3; 5); G3 = (0.3; 12); G4 = (0.35; 24); G5 = (0.35; 16); G6 = (0.25; 15); G7 = (0.3; 20); G8 = (0.35; −8). Phase cycle: $\phi 1 = 2(x), 2(-x)$; $\phi 2 = 2(45°), 2(225°)$; $\phi 3 = y, -y$; $\phi 4 = x$ in experiment (1) and $-x$ in experiment (2), $\phi 5 = 45°$; $\phi 6 = x$; $\phi 7 = 2(x), 2(-x)$; rec. $= 2(x), 2(-x)$. Quadrature detection in t_1 is achieved via a gradient enhanced sensitivity scheme: for each t_1 value a pair of spectra are recorded with ($\phi 5$; $\phi 6$) = (x; G8) and ($\phi 5$; $\phi 6$) = ($-x$; −G8) and manipulated in a post-acquisition manner (Kay et al. 1992; Schleucher et al. 1993). The phase $\phi 1$ is inverted for each t_1 point (Marion et al. 1989)

^{1}H–^{15}N splittings measured in F_1 from the combination of TROSY and ^{1}H-decoupled spectra provide $^1J_{\mathrm{NH}}$ and ($^1J_{\mathrm{NH}} + ^1D_{\mathrm{NH}}$) values scaled by a factor of 2, so that $^1J_{\mathrm{NH}}/2$ and ($^1J_{\mathrm{NH}} + ^1D_{\mathrm{NH}}$)/2 are effectively quantified. It can be shown that this scaling factor is close to being optimal for the measurements of $^1J_{\mathrm{NH}}(^1D_{\mathrm{NH}})$ couplings in MSG (isotropic $\tau_C \approx 37$ ns at 37°C (Tugarinov et al. 2002)). For example, earlier measurements of $^1J_{\mathrm{NH}}(^1D_{\mathrm{NH}})$ couplings in MSG have been performed using a 3D '*J*-scaled' TROSY-HNCO-based pulse-scheme (Tugarinov and Kay 2003; Kontaxis et al. 2000; Yang et al. 1999), where ^{1}H decoupling is employed during constant-time ^{15}N evolution period, leading to reduction of ^{15}N–^{1}H splittings by the same factor of 2. ^{1}H decoupling with the hard 180° pulse in the middle of t_1 period in experiment 2 of Fig. 1 is equivalent to setting the *J* scaling parameter (α) to zero in the constant-time ^{15}N evolution period of the *J*-scaled TROSY-HNCO scheme. As it has been shown by Kontaxis et al. (2000) that the optimal value of the scaling parameter α is achieved when $exp(-(1 + \alpha)T_{\mathrm{N}}R_2) \approx 0.2$, where T_{N} is ½ of the constant-time evolution period and R_2 is the relaxation rate of the fast-relaxing (up-field) component of the ^{15}N doublet. Using $T_{\mathrm{N}} = 16.8$ ms as in TROSY-HNCO, $R_2 \approx 100\ \mathrm{s}^{-1}$ (approximate value estimated for MSG at 37°C) and $\alpha = 0$ we obtain $exp(-(1 + \alpha)T_{\mathrm{N}}R_2) = 0.18$—very close to the optimal value. Figure 2 shows a superposition of selected regions of amide (Fig. 2a) and methyl (Fig. 2b) portions of the simultaneous ^{1}H–^{15}N/^{1}H$_m$–^{13}C$_m$ correlation map used for $^1D_{\mathrm{NH}}(^1D_{\mathrm{CH}})$ measurements from the differences in $F_1(F_2)$ splittings obtained in ^{1}H-decoupled/(IP-AP) spectra (red contours) and TROSY/(IP + AP) spectra (black contours) of {U-[^{15}N,^{2}H]; Ileδ1-[^{13}CH$_3$]; Leu,Val-[^{13}CH$_3$/^{12}CD$_3$]}-labeled MSG. The ^{1}H-^{15}N splittings obtained in F_1 should be doubled for the derivation of couplings.

Recently, we have reported accurate measurements of methyl $^1D_{\mathrm{CH}}$ and $^1D_{\mathrm{CC}}$ RDCs in ILV-protonated samples of MSG using a 3D approach that allows dispersion of methyl correlations to the third ($^{13}C^{\beta/\gamma}$) dimension alleviating the problem of overlap of resonances in methyl-abundant large proteins (Guo et al. 2010). A good agreement was observed between the measured RDCs of both types and those calculated from the crystallographic coordinates of MSG for the subset of methyl sites with

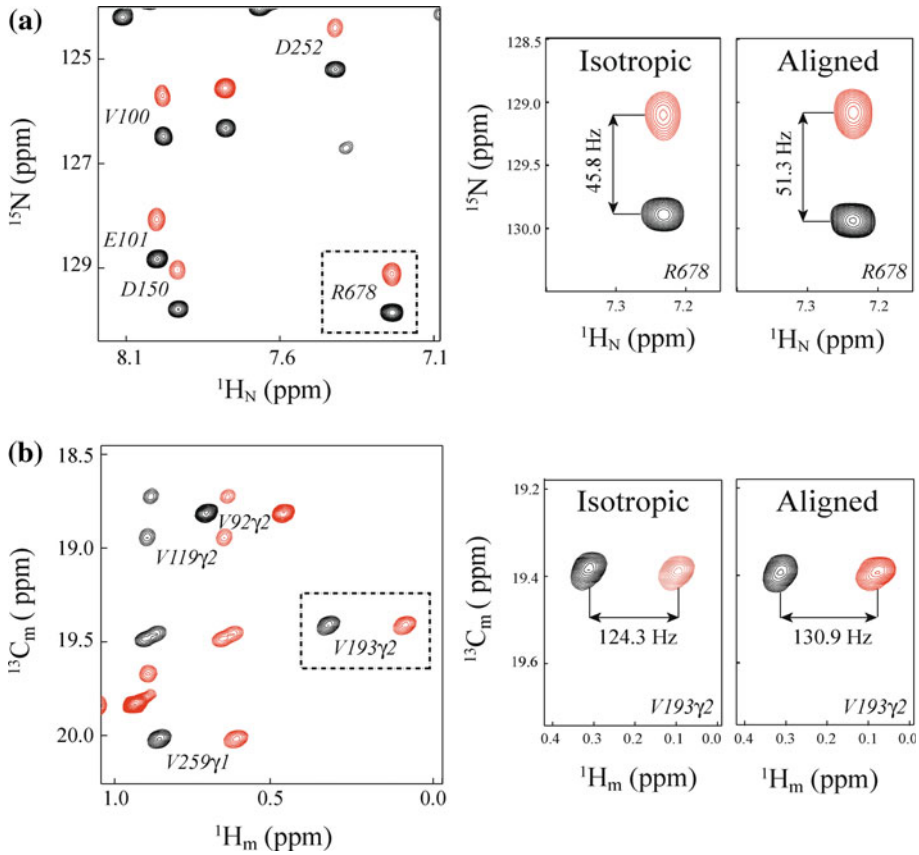

Fig. 2 Superposition of selected regions of simultaneous ^{1}H–^{15}N/^{1}H$_m$–^{13}C$_m$ correlation maps with ^{1}H-decoupled/(IP-AP) spectra (shown with *red contours*), and TROSY/(IP + AP) (*black contours*) in isotropic and aligned samples of {U-[^{15}N,^{2}H]; Ileδ1-[^{13}CH$_3$]; Leu,Val-[^{13}CH$_3$/^{12}CD$_3$]}-labeled MSG (0.7 mM; 37°C; 600 MHz; 90% H_2O/10% D_2O) using the pulse scheme in Fig. 1. **a** Amide ^{1}H-^{15}N region used for $^{1}D_{NH}$ RDC, and **b** Leu-Val methyl region used for $^{1}D_{CH}$ RDC measurements. The regions enclosed in *dashed rectangles* in (**a**) and (**b**) are enlarged to the right of each plot. The sample of MSG was dissolved in 25 mM sodium phosphate buffer (pH = 7.1) containing 5 mM DTT; 0.05% NaN_3; 20 mM $MgCl_2$. MSG was oriented in pf1 phage (~12 mg/ml; Hansen et al. 1998)

low-amplitude internal dynamics (high values of the methyl threefold axis order parameter, S_{axis}) using the parameters of the alignment tensor established for MSG earlier under identical experimental conditions (Tugarinov and Kay 2003): ($A_a = -1.6e-3$; $R = 0.4$; $\alpha = 7°$; $\beta = 133°$; $\gamma = 243°$), where A_a and R are axial and rhombic components of the alignment tensor, and the Euler angles (α; β; γ) describe the orientation of the principal axes with respect to the PDB frame of glyoxylate-bound MSG (PDB code 1d8c (Howard et al. 2000)). Therefore, subsequently it came as a surprise to observe that in a number of other selectively ILV-[^{13}C,^{1}H]-labeled samples of MSG, the correlation between $^{1}D_{CH}$ couplings (measured in D_2O using the 2D HMQC-IPAP scheme of (Sprangers and Kay 2007)) and MSG structure could not be reproduced even though the same experimental conditions—at least those that can be controlled, such as buffer composition, ionic strength, pH, concentration of pf1 phage resulting in the same ^{2}H splitting in HDO signal to within 0.1–0.2 Hz—have been used in all experiments. The source of these discrepancies could be traced to a substantial variation of the alignment tensor of MSG in these pf1-phage oriented samples.

Despite the fact that identical sample conditions were used in all the cases, the fitting of $^{1}D_{NH}$ RDCs measured using the scheme of Fig. 1 in a number of MSG samples provided alignment tensor parameters significantly different from the values above: $A_a = 1.02e-3$; $R = 0.4$; $\alpha = 53°$; $\beta = 50°$; $\gamma = 61°$. Figures 3a, b show correlation plots between experimental and calculated $^{1}D_{NH}$ values for the same subset of 119 amides obtained earlier from the '*J*-scaled' 3D TROSY-HNCO spectra using original alignment parameters (Fig. 3a), and from the present simultaneous 2D $^{1}D_{NH}$ and $^{1}D_{CH}$ measurements using the alignment tensor parameters $A_a = +1.02e-3$; $R = 0.4$; $\alpha = 53°$; $\beta = 50°$; $\gamma = 61°$ (Fig. 3b). The agreement is comparable although very different alignment parameters have been used for the two calculations. The normalized scalar product between the directors of the two tensors is equal to 0.2. Standard errors in $^{1}D_{NH}$($^{1}D_{CH}$) RDCs estimated from duplicate measurements are 2.8(0.8) Hz, while back-calculated RDCs from the fitting of duplicate $^{1}D_{NH}$($^{1}D_{CH}$) sets have pair-wise r.m.s.d of only 0.6(0.2) Hz. Using Monte-Carlo simulations with these standard errors we estimate that the uncertainties in the derived alignment parameters of MSG are [0.04×10^{-3}; 0.03; 1.4°; 1.0°; 2.5°] for [A_a; R; α; β; γ]. Very similar alignment parameters have been obtained using the coordinates of the ternary pyruvate–acetyl–CoA-MSG complex (PDB code 1p7t (Anström et al. 2003)) indicating that the errors in

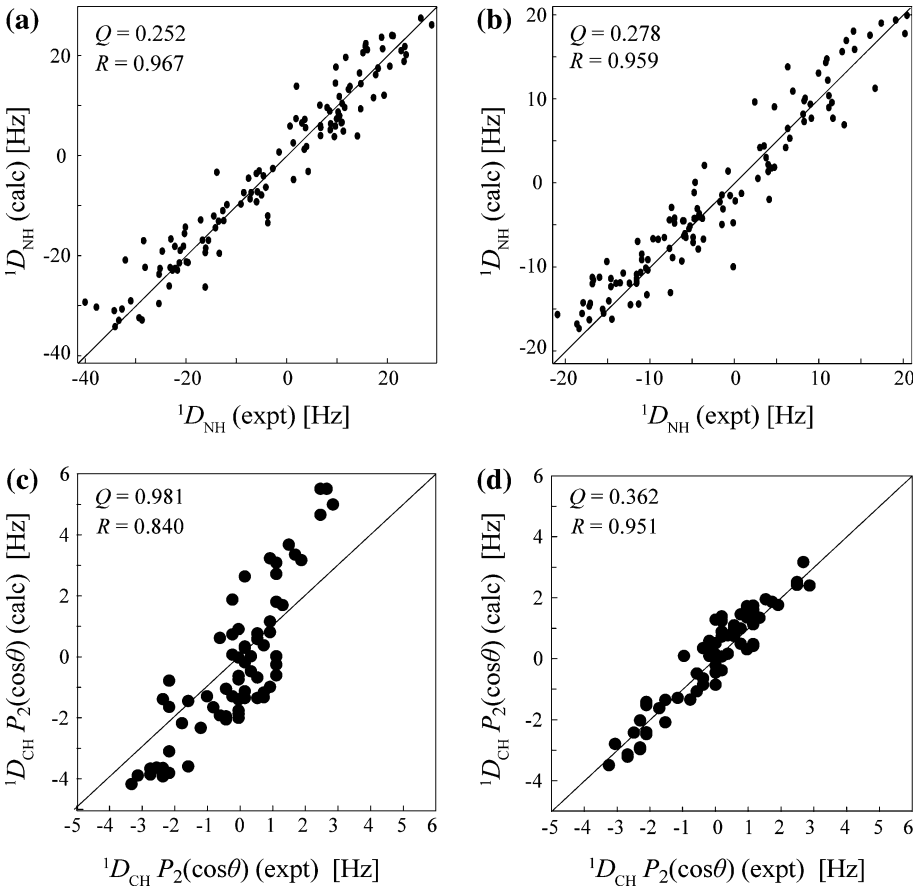

Fig. 3 Correlations between experimental and calculated $^1D_{NH}$ and methyl $^1D_{CH}$ RDCs in MSG. **a–b** A correlation plot between experimental and calculated $^1D_{NH}$ values for the same subset of 119 amides obtained from **a** the data of Tugarinov and (Kay 2003) using the alignment tensor parameters ($A_a = -1.6e-3$; $R = 0.4$; $\alpha = 7°$; $\beta = 133°$; $\gamma = 243°$), and **b** simultaneous 2D $^1D_{NH}$ and $^1D_{CH}$ RDC measurements using the alignment tensor parameters ($A_a = 1.02e-3$; $R = 0.4$; $\alpha = 53°$; $\beta = 50°$; $\gamma = 61°$). **c–d** Correlation plots between experimental and calculated methyl $^1D_{CH}$ RDCs for the subset of 72 values obtained using the alignment parameters (**c**) as in **a**, and **d** as in **b**. All $^1D_{CH}$ values are pre-multiplied with $P_2(\cos\theta)$, where θ is the C–C–H dihedral angle in a methyl group (110.8°), (Mittermaier and Kay 2002; Ottiger and Bax 1999) and $P_2(x) = 0.5[3x^2 - 1]$. The program PIPP (Garrett et al. 1991) was used for accurate measurements of peak positions in the spectra. The coordinates of amide ^{1}H–^{15}N and methyl axis C_m–C bond vectors have been obtained from the *x*-ray structure of glyoxylate-bound MSG [PDB code 1d8c (Howard et al. 2000)]. *Solid lines* correspond to $y = x$

alignment parameters are primarily of experimental nature and do not arise from 'structural noise'.

It has been demonstrated on a number of occasions previously that simple scaling of methyl $^1D_{CH}$ RDCs with $\sqrt{(S^2_{axis})}$ can be a reasonable approximation for a semi-quantitative interpretation of methyl RDCs in the side-chains with low amplitude dynamics (Guo et al. 2010; Ottiger et al. 1998a, b; Sprangers and Kay 2007). Here, we concentrated on the subset of methyls for which (1) crystallographic coordinates are available (Howard et al. 2000), (2) stereospecific assignments of Val(Leu) $\gamma(\delta)$ methyls have been obtained (Tugarinov and Kay 2004), (3) whose S_{axis} is available and exceeds 0.84 as derived earlier from ^{13}C relaxation measurements in $^{13}CHD_2$ methyls of MSG (Tugarinov and Kay 2005), and (4) whose $^1D_{CH}$ values are reproducible to within standard errors in MSG samples with different protein concentrations (see below). Figures 3c, d show correlation plots between experimental and calculated $^1D_{CH}$ RDCs measured for the same subset of 72 methyl sites from the 2D SIM-$^{13}C_m$–^1H_m/^{1}H–^{15}N experiment using original alignment parameters (Fig. 3c), and using the alignment tensor derived from $^1D_{NH}$ RDCs measured from the 2D SIM-$^{13}C_m$–^1H_m/^{1}H–^{15}N data set (Fig. 3d). Clearly, the right choice of the alignment tensor parameters significantly affects the quality of $^1D_{CH}$ correlations.

In search of the sources of the observed variation in the alignment tensor characteristics, we have eliminated a number of possibilities. Exactly the same sample conditions have been used in all the previous and present measurements including (1) buffer composition of NMR samples, (2) pH(pD), (3) the concentration of $MgCl_2$, and

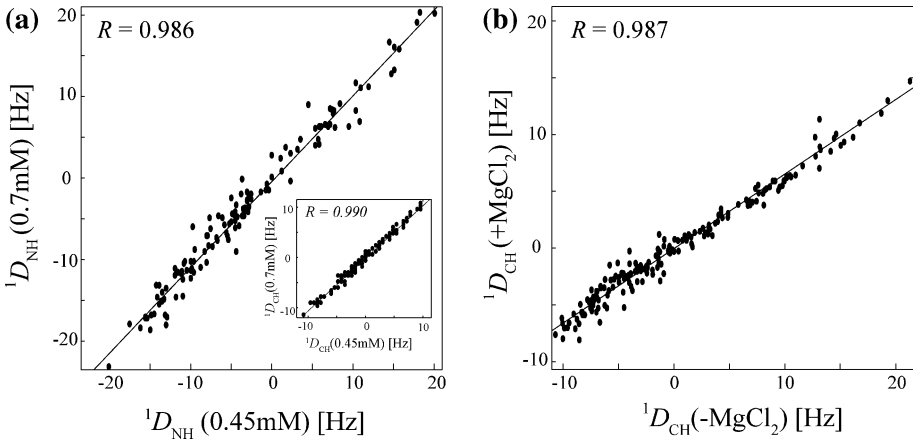

Fig. 4 Correlation plots of $^1D_{NH}$ and $^1D_{CH}$ RDCs measured in MSG using the scheme of Fig. 1 with different sample conditions. **a** Correlation plot between of $^1D_{NH}$ RDCs measured for a subset of 129 amides in MSG samples with 0.45 mM (*x*-axis) and 0.7 mM (*y*-axis) protein concentrations. The *solid line* represents linear regression fit of the data with a slope of 1.04 and the intercept of −0.25. Pearson $R = 0.986$. The *inset* shows the correlation between 175 methyl $^1D_{CH}$ RDCs obtained for the same sample concentrations; **b** correlation plot between $^1D_{CH}$ RDCs measured for a subset of 175 methyl groups of MSG without $MgCl_2$ (*x*-axis) and with 20 mM $MgCl_2$ (*y*-axis). The *solid line* represents linear regression fit of the data with a slope of 0.65 and the intercept of −0.06. Pearson $R = 0.987$

(4) the concentration of pf1 phage. The solvent ^2H splitting in different samples varied in the narrow range between 9.9 and 10.1 Hz. Using the scheme of Fig. 1, $^1D_{NH}$ and $^1D_{CH}$ RDCs have been measured in the samples with varying protein concentrations in the range between 0.4 and 1.0 mM. Figure 4a shows correlations between of $^1D_{NH}$ and $^1D_{CH}$ couplings measured for a subset of 129 amides and 175 ILV methyls in the samples containing 0.45 and 0.7 mM protein solutions. A good agreement between the two sets of couplings (the slope of 1.04 and Pearson $R = 0.986$) indicates that protein concentration does not significantly affect alignment. Finally, slight precipitation of magnesium phosphate from the sodium phosphate buffer containing $MgCl_2$ over the time of NMR measurements would result in lower concentration of $MgCl_2$ in solution. Nevertheless, this would only increase alignment in pf1 phage, whereas the observed alternative alignment tensor is smaller in absolute magnitude ($A_a = 1.02e-3$ vs. $A_a = -1.6e-3$ derived previously) and has a different orientation. Figure 4b shows a correlation plot between $^1D_{CH}$ RDCs obtained in the samples of MSG in the absence of $MgCl_2$ and with 20 mM $MgCl_2$ (measured separately in D_2O using the 2D HMQC-IPAP scheme). Indeed, the couplings obtained in the presence of 20 mM $MgCl_2$ are smaller by ~35% indicating *weaker* alignment resulting from higher ionic strength—in agreement with existing experimental and theoretical predictions for alignment in pf1 phage (Zweckstetter and Bax 2001; Zweckstetter et al. 2004). High correlation of the two sets of couplings in Fig. 4b also indicates that the changes due to differences in ionic strength are restricted to A_a and do not significantly affect the orientation of the tensor. However, as shown in Fig. 5a, b, the orientations of the two alternative alignment tensors of MSG are significantly different.

The only possible explanation for the observed variation in alignment parameters might involve the quality and homogeneity of pf1 phage preparations that may deteriorate with time. Although this was not verified in a systematic way in this work, the comparison of agarose gels of the newly prepared pf1 phage and that stored for prolonged periods of time showed some deterioration in its homogeneity and possible fragmentation of phage particles. We therefore hypothesize that the patches of positively charged residues on the surface of the protein (shown in Fig. 5c) might be involved in somewhat stronger electrostatic interactions with negatively charged phage particles when pf1 phage gets partially degraded. Of note, the variation of the alignment parameters observed in MSG is reminiscent of the alignment variation in the protein GB1 as a function of ionic strength (Zweckstetter et al. 2004)—namely, smaller absolute values of A_a and the change in its sign, practically the same rhombicity R, and a different orientation of the tensor at higher (>200 mM) NaCl concentrations—although no salt was used in MSG samples besides 20 mM $MgCl_2$ and sodium phosphate. Irrespective of the reasons for the observed variation in alignment, the 2D SIM-$^{13}C_m$–^1H_m/^1H–^{15}N experiment for simultaneous measurements of $^1D_{CH}$ and $^1D_{NH}$ couplings described here provides convenient means of verification of the alignment parameters in large {U-[^{15}N,^2H]; Ileδ1-[$^{13}CH_3$]; Leu,Val-[$^{13}CH_3$/$^{12}CD_3$]}-labeled proteins where

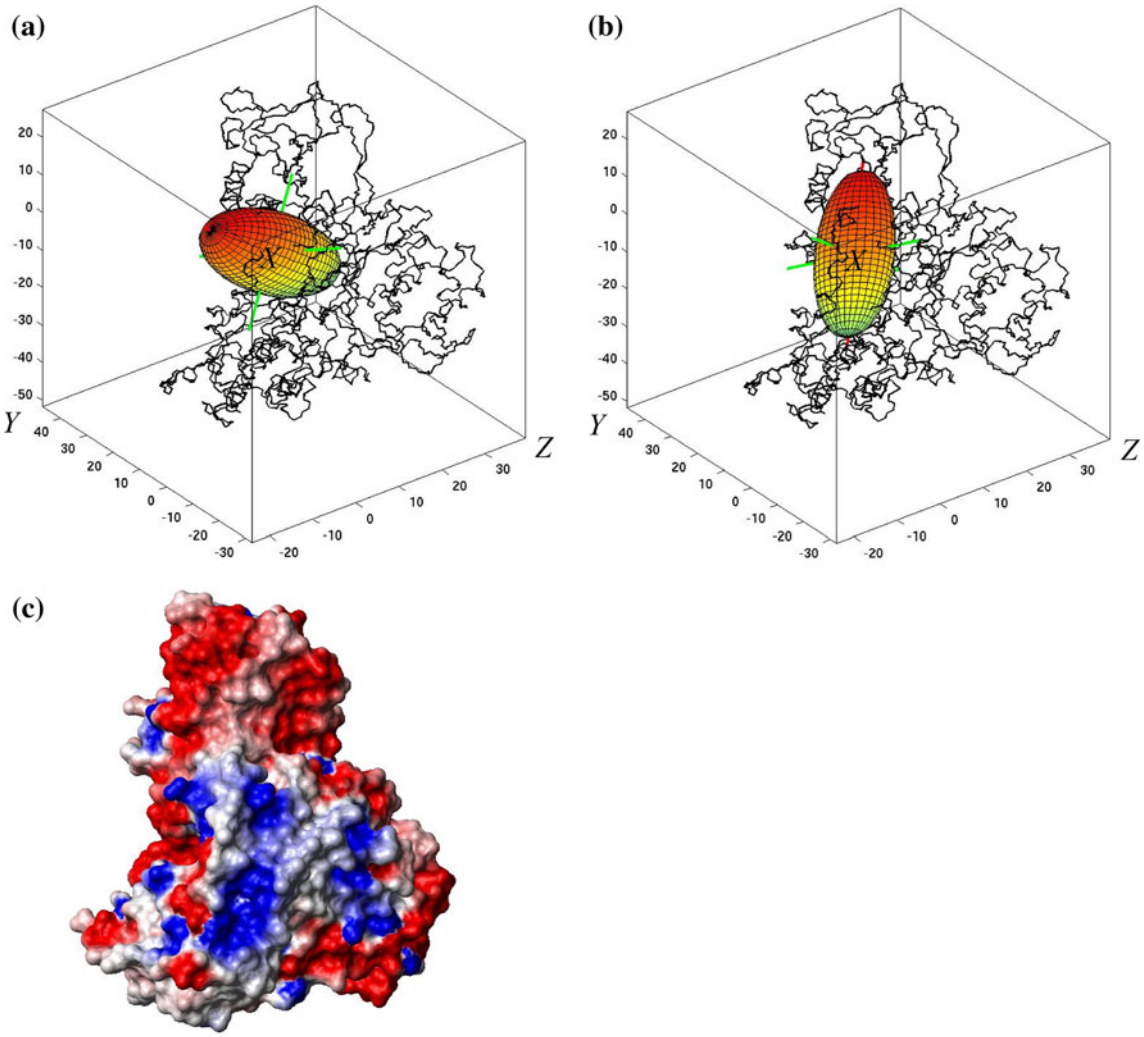

Fig. 5 Orientation of alignment tensors obtained from $^{1}D_{NH}$ RDCs in MSG with respect to the frame of crystallographic coordinates (PDB frame) **a** in (Tugarinov and Kay 2003): the Euler angles $\alpha = 7°$; $\beta = 133°$; $\gamma = 243°$, and **b** in this work: $\alpha = 53°$; $\beta = 50°$; $\gamma = 61°$. **c** Surface representation of the MSG structure shown in the same orientation as in **a**–**b**. Negatively (positively)-charged areas are shown in *red* (*blue*)

methyl $^{1}D_{CH}$ couplings in ordered side-chains are sought to be interpreted in terms of structure.

Acknowledgments The authors thank Prof. W.-Y. Choy (University of Western Ontario, Canada) for the program RDCA2.0 used to fit and visualize alignment tensors derived from $^{1}D_{NH}$ couplings, and Prof. Joel Tolman (Johns Hopkins University, Maryland) for useful discussions.

References

Anström DM, Kallio K, Remington SJ (2003) Structure of the *Escherichia coli* malate synthase G:pyruvate:acetyl-coenzyme a abortive ternary complex at 1.95 a resolution. Protein Sci 12:1822–1832

Bax A, Kontaxis G, Tjandra N (2001) Dipolar couplings in macromolecular structure determination. Methods Enzymol 339:127–174

Boyd J, Soffe N (1989) Selective excitation by pulse shaping combined with phase modulation. J Magn Reson 85:406–413

Garrett DS, Powers R, Gronenborn AM, Clore GM (1991) A common sense approach to peak picking in two-, three-, and four-dimensional spectra using automatic computer analysis of contour diagrams. J Magn Reson 95:214–220

Geen H, Freeman R (1991) Band-selective radiofrequency pulses. J Magn Reson 93:93–141

Godoy-Ruiz R, Guo C, Tugarinov V (2010) Alanine methyl groups as NMR probes of molecular structure and dynamics in high-molecular-weight proteins. J Am Chem Soc 132:18340–18350

Guo C, Tugarinov V (2009) Identification of HN-methyl NOEs in large proteins using simultaneous amide-methyl TROSY-based detection. J Biomol NMR 43:21–30

Guo C, Zhang D, Tugarinov V (2008) An NMR experiment for simultaneous TROSY-based detection of amide and methyl groups in large proteins. J Am Chem Soc 130:10872–10873

Guo C, Godoy-Ruiz R, Tugarinov V (2010) High resolution measurement of methyl $^{13}C_m$–^{13}C and $^{1}H_m$–$^{13}C_m$ residual

dipolar couplings in large proteins. J Am Chem Soc 132:13984–13987
Hansen MR, Mueller L, Pardi A (1998) Tunable alignment of macromolecules by filamentous phage yields dipolar coupling interactions. Nat Struct Biol 5:1065–1074
Howard BR, Endrizzi JA, Remington SJ (2000) Crystal structure of *Escherichia coli* malate synthase G complexed with magnesium and glyoxylate at 2.0. A resolution: mechanistic implications. Biochemistry 39:3156–3168
Kay LE, Keifer P, Saarinen T (1992) Pure absorption gradient enhanced heteronuclear single quantum correlation spectroscopy with improved sensitivity. J Am Chem Soc 114:10663–10665
Kontaxis G, Clore GM, Bax A (2000) Evaluation of cross-correlation effects and measurement of one-bond couplings in proteins with short transverse relaxation times. J Magn Reson 143:184–196
Marion D, Ikura M, Tschudin R, Bax A (1989) Rapid recording of 2D NMR spectra without phase cycling. Application to the study of hydrogen exchange in proteins. J Magn Reson 85:393–399
Mittermaier A, Kay LE (2002) Effect of deuteration on some structural parameters of methyl groups in proteins as evaluated by residual dipolar couplings. J Biomol NMR 23:35–45
Nuzillard JM, Freeman R (1994) Oversampling in two-dimensional NMR. J Magn Reson A 110:252–258
Ottiger M, Bax A (1999) How tetrahedral are methyl groups in proteins? A liquid crystal NMR study. J Am Chem Soc 121:4690–4695
Ottiger M, Delaglio F, Bax A (1998a) Measurement of J and dipolar couplings from simplified two-dimensional NMR spectra. J Magn Reson 131:373–378
Ottiger M, Delaglio F, Marquardt JL, Tjandra N, Bax A (1998b) Measurement of dipolar couplings for methylene and methyl sites in weakly oriented macromolecules and their use in structure determination. J Magn Reson 134:365–369
Patt SL (1992) Single- and multiple-frequency-shifted laminar pulses. J Magn Reson 96:94–102
Pervushin K, Riek R, Wider G, Wüthrich K (1997) Attenuated T_2 relaxation by mutual cancellation of dipole-dipole coupling and chemical shift anisotropy indicates an avenue to NMR structures of very large biological macromolecules in solution. Proc Natl Acad Sci USA 94:12366–12371
Pervushin KV, Wider G, Wüthrich K (1998) Single transition to single transition polarization transfer (ST2-PT) in [^{15}N, ^{1}H]-TROSY. J Biomol NMR 12:345–348
Prestegard JH (1998) New techniques in structural NMR—anisotropic interactions. Nat Struct Biol NMR Suppl 5:517–522
Schleucher J, Sattler M, Griesinger C (1993) Coherence selection by gradients without signal attenuation: application to the three-dimensional HNCO experiment. Angew Chem Intl Ed Engl 32:1489–1491
Sprangers R, Kay LE (2007) Probing supramolecular structure from measurement of methyl ^{1}H–^{13}C residual dipolar couplings. J Am Chem Soc 24:12668–12669
Tjandra N, Bax A (1997) Direct measurement of distances and angles in biomolecules by NMR in a dilute liquid crystalline medium. Science 278:1111–1114
Tolman JR, Flanagan JM, Kennedy MA, Prestegard JH (1995) Nuclear magnetic dipole interactions in field-oriented proteins: information for structure determination in solution. Proc Natl Acad Sci USA 92:9279–9283
Tugarinov V, Kay LE (2003) Quantitative NMR studies of high molecular weight proteins: application to domain orientation and ligand binding in the 723-residue enzyme malate synthase G. J Mol Biol 327:1121–1133
Tugarinov V, Kay LE (2004) Stereospecific NMR assignments of prochiral methyls, rotameric states and dynamics of valine residues in malate synthase G. J Am Chem Soc 126:9827–9836
Tugarinov V, Kay LE (2005) Quantitative ^{13}C and ^{2}H NMR relaxation studies of the 723-residue enzyme malate synthase G reveal a dynamic binding interface. Biochemistry 44:15970–15977
Tugarinov V, Muhandiram R, Ayed A, Kay LE (2002) Four-dimensional NMR spectroscopy of a 723-residue protein: chemical shift assignments and secondary structure of malate synthase G. J Am Chem Soc 124:10025–10035
Tugarinov V, Hwang PM, Ollerenshaw JE, Kay LE (2003) Cross-correlated relaxation enhanced ^{1}H–^{13}C NMR spectroscopy of methyl groups in very high molecular weight proteins and protein complexes. J Am Chem Soc 125:10420–10428
Velyvis A, Schachman HK, Kay LE (2009) Application of methyl-TROSY NMR to test allosteric models describing effects of nucleotide binding to aspartate transcarbamoylase. J Mol Biol 387:540–547
Yang D, Kay LE (1999) Improved 1HN-detected triple resonance TROSY-based experiments. J Biomol NMR 13:3–10
Yang D, Nagayama K (1996) A sensitivity-enhanced method for measuring heteronuclear long-range coupling constants from the displacement of signals in two 1D subspectra. J Magn Reson Ser A 118:117–121
Yang D, Venters RA, Mueller GA, Choy WY, Kay LE (1999) Trosy-based HNCO pulse sequences for the measurement of ^{1}HN–^{15}N, ^{15}N–^{13}CO, ^{1}HN–^{13}CO, ^{13}CO–^{13}Cα dipolar couplings in ^{15}N, ^{13}C, ^{2}H-labeled proteins. J Biomol NMR 14:333–343
Zweckstetter M, Bax A (2001) Characterization of molecular alignment in aqueous suspensions of Pf1 bacteriophage. J Biomol NMR 20:365–377
Zweckstetter M, Hummer G, Bax A (2004) Prediction of charge-induced molecular alignment of biomolecules dissolved in dilute liquid-crystalline phases. Biophys J 86:3444–3460